THE JOURNAL OF PHYSICAL CHEMISTRY C
A JOURNAL OF THE AMERICAN CHEMICAL SOCIETY

pubs.acs.org/JPCC
Article

Investigation on the Structure–Function Relationship of Atomic-Layer-Deposited Platinum Additives on Tungsten Trioxide Gas Sensor Materials

David Degler, Ugur Geyik, Benjamin Junker-Reiss, Muhammad Hamid Raza, Patrick Amsalem, Norbert Koch, Blanka Detlefs, Nicola Pinna, Udo Weimar, and Nicolae Barsan*

Cite This: J. Phys. Chem. C 2025, 129, 15301−15308

Read Online

ACCESS | Metrics & More | Article Recommendations | Supporting Information

ABSTRACT: Different Pt structures were deposited on WO_3 by using atomic layer deposition. The gas sensing properties, structures of the Pt loadings, and their influence on the gas detection mechanism were investigated using extensive material characterization and operando spectroscopies. The results show that, depending on the number of atomic layer deposition cycles, different Pt structures can be obtained, which influence the gas detection in different ways. The found structures range from predominantly ionic Pt sites over oxidic particles to partially oxidized metallic particles. It was found that single ion sites and small oxidic particles have the most effective influence on gas detection, whereas partially oxidized metal particles lead to a lower gas sensing performance.

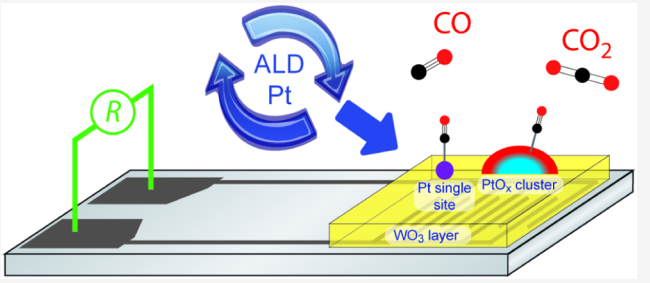

INTRODUCTION

Chemoresistive gas sensors based on semiconducting metal oxides (SMOX) are used in a wide variety of applications, ranging from air quality measurements over process control to health or safety applications.[1−3] The detection of the analyte gases takes place by different surface reactions and strongly depends on the nature of the SMOXs' surface properties, the analyte gas as such, and other gases present. For WO_3, these surface reactions range from the interplay of reduction and reoxidation of the SMOX surface by analyte gases like CO or H_2 to complex reactions involving dehydrogenation and partial oxidation, as observed for different volatile organic compounds.[4−8] If at least one step of these surface reactions involves a charge transfer between SMOX and reactive surface species, this interplay has a direct influence on the number of free charge carriers and, thus, on sensor resistance, i.e., the sensor signal.[2,9] Both the electrical properties of the SMOX bulk or surface and the reactivity of the surface can be strongly influenced by the deposition of noble metal additives at the surface. Their composition, structure, and distribution on the supporting SMOX have a significant influence on the gas sensing properties.[10,11] The structures of noble metal loadings range from individual atoms or ions, which can form a reactive center, to the introduction of separate noble metal phases that form a heterojunction. In addition to this size effect, the coverage of the SMOX and distribution of the noble metal loading also play an essential role. If there is too little noble metal present or if it is poorly distributed, this only has a local influence on the chemical and, in particular, electrical properties, i.e., it changes the reactivity, but not sufficiently the charge transport and thus the gas-sensitive properties.[11]

A difficulty in previous studies was to separate the influence of different synthesis methods on the nature and size of the noble metal additives and the SMOX as such from size-dependent changes in the gas sensing mechanism. In order to determine structure−function relationships, it is therefore of great importance to be able to obtain noble metal structures of different sizes using the same synthesis method. Thus, atomic layer deposition (ALD) was selected as the synthesis method of choice for this study, as it allows precise control over the deposition process and can be applied to already prepared gas sensors devices, i.e., eliminating possibly negative impacts of the sensing layer deposition on the noble metal additives, and focuses Pt deposition to regions accessible to the target and interfering gases.[12,13]

For this investigation targeting the effect of Pt surface additives, it makes sense to choose a target gas that has a simple surface chemistry. The logical choice is CO, whose surface chemistry on WO_3 is well understood.[6,7] Furthermore, unlike H_2, CO does not form hydroxyl groups. Also it does not undergo

Received: July 18, 2025
Revised: August 7, 2025
Accepted: August 7, 2025
Published: August 15, 2025

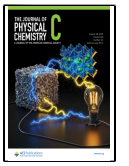

https://doi.org/10.1021/acs.jpcc.5c05000
J. Phys. Chem. C 2025, 129, 15301−15308

complex surface reactions, as is the case with volatile organic compounds.

MATERIALS AND METHODS

WO_3 nanoparticles were purchased from Sigma-Aldrich (Sigma-Aldrich Co., <100 nm particle size), and trimethyl-(methylcyclopentadienyl)platinum(IV) [(MeCp)Pt(IV)Me_3], 99%, was purchased from STREM Chemicals Inc. The gases for the synthesis (Ar, O_2, N_2) were sourced from Air Liquide, and all had a purity of 99.99%. For gas sensing and operando experiments, the carrier gases (synthetic air, N_2, or He) and high-purity test gas mixtures were obtained from Westfalen, with the exception of the experiments done at the synchrotron light source, where on-site available high-purity carrier gases and analyte mixtures were used.

Gas sensors were produced by screen-printing a 1,2-propanediol-based WO_3 paste onto planar Al_2O_3 substrates, which are equipped with interdigitated Pt electrodes on the front and a backside Pt heater.[14] The coated gas sensors were dried at 70 °C and calcined stepwise at 400, 500, and 400 °C for 10 min each. For X-ray absorption and X-ray photoelectron spectroscopies, special Al_2O_3 substrates with Au electrodes and a Pd/Ag-alloy heater were used to avoid Pt signals from the sensor substrate.

Pt loadings were deposited on WO_3 directly onto the calcined gas sensors. ALD was performed in a thermal ALD system by ARRADIANCE (GEMStar-XT). [(MeCp)Pt(IV)Me_3], contained in a stainless steel canister at 55 °C, and ultrahigh purity O_2 were used as metal precursor and counter-reactant/oxidant, respectively. The precursors were supplied using two separate supply lines maintained at 120 °C and 80 °C for the platinum precursor and oxygen, respectively. N_2 was used as a carrier gas and purging gas for the precursors to the reaction chamber, and to remove any of the excess reactants and byproducts, respectively. The temperature of the ALD reaction chamber was maintained at 265 °C during Pt deposition. The ALD cycle was adjusted as a pulse/exposure/purge sequence of 0.6/30/30 s and 0.3/35/50 s for (MeCp)Pt(IV) Me_3 and O_2, respectively. The nature, loading, and the particle size of the Pt species were controlled by changing the number of ALD cycles (2, 5, 10, 25, and 50). The samples are named ALD2, ALD5, ALD10, ALD25, and ALD50, respectively. The ALD process was followed by calcination at 300, 400, 500, and 400 °C for 10 min each.

X-ray photoelectron spectroscopy (XPS) measurements were performed using JPS-9030 (JEOL) and Phoibos 100 (SPECS) hemispherical analyzers in ultrahigh vacuum (UHV) setups (base pressure 5×10^{-10} mbar) and the Mg Kα radiation from dual anode X-ray sources.

High-angle annular dark-field scanning transmission electron microscopy (HAADF-STEM) was performed using a FEI Talos F200S scanning/transmission electron microscope operated at 200 kV. The analysis of the microscopy data was performed using Velox software, version 2.6, and *ImageJ* freeware.

For gas sensing and operando spectroscopy, gases were mixed and dosed using a homemade gas mixing system based on computer-controlled mass flow controllers. Relative humidity (RH) levels were adjusted by mixing humidified air from a bubbler filled with deionized water at 20 °C in the dry gas stream. Gas sensors were placed in dedicated measuring cells, and the heaters were connected to a power supply. The sensor resistance was recorded using a digital electrometer (Keithley 617).

X-ray absorption spectroscopy (XAS) was performed at X-ray absorption and emission spectroscopy beamline ID26 at the European Synchrotron Radiation Facility (ESRF) in Grenoble, France. The incident energy was selected using a double-crystal monochromator with a Si(111) crystal, with an energy resolution of 1.75 eV. High-energy-resolved fluorescence detection (HERFD) was used to record X-ray absorption near edge structure (XANES) spectra at the Pt L_3 edge (Pt $L_{\alpha 1}$ emission line) as a function of the incident energy using a Johann geometry X-ray emission spectrometer, equipped with four Ge crystal analyzers (Ge(660) reflection).[15] The use of HERFD is necessary to detect traces of Pt in the presence of W, as the overlap of the Pt $L_{\alpha 1}$ (9442 eV) and W $L_{\beta 1}$ (9472 eV) emission lines prevents other detection methods, due to the large excess of W in the WO_3 support. The HERFD-XANES spectra were evaluated using the Larch software package.[16]

Diffuse reflectance infrared Fourier transform spectroscopy (DRIFTS) was carried out on a Vertex 70v spectrometer (Bruker) equipped with a high-performance globar mid-IR source and a midband MCT detector. The sensors were placed in a homemade operando cell with a KBr window, which was fixed in a six-mirror optic (Praying Mantis by Harrick). DRIFT spectra were recorded with a resolution of 2 cm^{-1}. Absorbance spectra were calculated as described elsewhere.[17]

RESULTS AND DISCUSSION

The composition of the Pt species at the surface was studied by XPS (Figure 1). The growing surface coverage of Pt with an increasing number of ALD cycles can be observed by comparing the intensities of the W 5s peak of WO_3 at 79.4 eV and the Pt 4f peaks at lower binding energies. The assignments of the different Pt binding energies are given in Table 1.

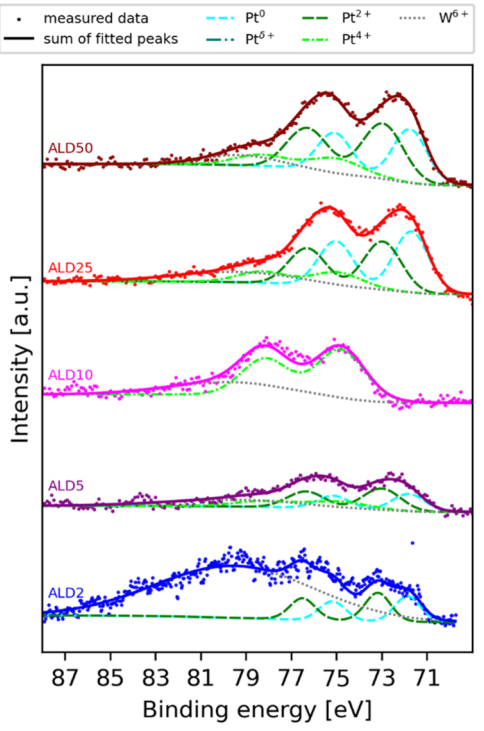

Figure 1. XP spectra of all Pt-loaded samples after calcination. The corresponding peak assignments are shown in Table 1. $Pt^{\delta+}$ was only found before calcination; see Figure S1.

https://doi.org/10.1021/acs.jpcc.5c05000
J. Phys. Chem. C 2025, 129, 15301−15308

Table 1. Assignment of Pt $4f_{7/2}$ Species Found by XPS

binding energy	species	assignment	references
71.1−71.3 eV	Pt^0	metallic Pt particles	18−22
72.0 eV	$Pt^{\delta+}$	single Pt atoms	23
72.7−73.0 eV	Pt^{2+}	single Pt ions	18,19,22
		partially oxidized Pt particles	19,20
74.8−75.0 eV	Pt^{4+}	Pt dioxide (PtO_2)	19,20

ALD2 shows the presence of a Pt^{2+} species, as well as metallic Pt. ALD5 shows a similar pattern of Pt^{2+} species and metallic Pt, but additionally a weak contribution of Pt^{4+}. ALD10 shows only the presence of Pt^{4+}. ALD25 and ALD50 show mainly metallic Pt and Pt^{2+} species with a contribution of Pt^{4+}.

To understand the impact of the calcination (400, 500, and 400 °C for 10 min each) on the Pt chemical state, i.e., the structure of the Pt loadings, additional spectra have been recorded prior to calcination (Figure S1). They clearly show different chemical states for the Pt surface species, depending on the number of ALD cycles. The change of single atom sites into other species due to calcination illustrates that single atom sites are not stable during sensor operation at 300 °C. Hence, a single treatment at an elevated temperature is required to obtain a sensor with a stable surface structure and, thus, performance.

To further investigate the morphology and microstructure of the Pt-loaded samples, HAADF-STEM was carried out before and after calcination. All micrographs of ALD2 (Figure 2) show

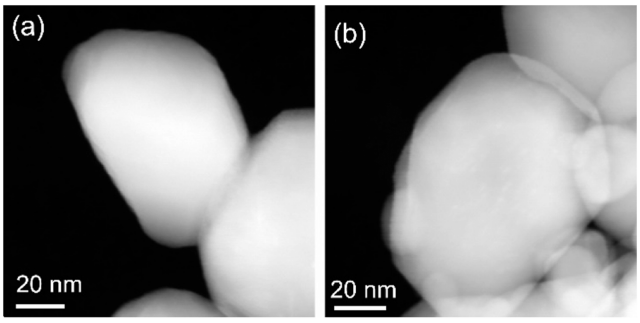

Figure 2. HAADF-STEM micrographs of ALD2 before (a) and after (b) calcination.

no phase that has segregated from the WO_3 particles, indicating the presence of single ionic Pt species, which are incorporated in the surface of WO_3, rather than metallic or oxidized Pt particles.[24]

For ALD5 to ALD50, electron microscopy reveals the presence of a separated phase both before (Figure S2) and after calcination (Figure 3), which is in agreement with the presence of fully metallic, fully oxidized, or partially oxidized Pt particles. The micrographs show that the WO_3 nanoparticles are uniformly covered with Pt clusters/particles, forming homogeneous particles at higher numbers of deposition cycles; the diameter of the Pt particles increases from around 1 nm for ALD5 to above 6 nm for ALD50. ALD50 shows agglomeration of the Pt particles, forming a quasi-continuous coverage of the supporting WO_3. This fine control of particle size is indeed one of the key features of the ALD method in combination with thermal treatment.[12,13]

As the chemical state of the Pt loadings is highly sensitive to the atmospheric composition and XPS and electron microscopy were done in vacuum, it is essential to probe the chemical state of the Pt loadings by an operando method, which allows to study the samples in realistic atmospheres and at typical operation conditions.[25] Thus, ALD2, ALD5, and ALD25 were selected to be further studied by operando XAS. Figure 4 shows the HERFD-XANES spectra of the three Pt-loaded WO_3 samples operated at 300 °C in the presence of 20% vol O_2 in a He background and reference spectra of Pt foil and PtO_2.

Comparing the Pt L_3 whiteline position of the ALD samples with the references clearly shows that on these samples, the loadings are present neither as metallic Pt nor as fully oxidized Pt^{4+}, but are rather found to be between the two references. In the literature, this is either assigned to Pt^{2+}, related to single Pt ions[18,22] or metallic Pt particles with an oxidized surface.[26] It is therefore not possible to distinguish between single Pt ions and partially oxidized particles using HERFD-XANES spectra. The differences in Pt L_3 whiteline intensities are expected to be real for ALD2 and ALD5, while for ALD25, the lower intensity may be caused by self-absorption due to the high Pt coverage. However, self-absorption should not affect the position of the whiteline and, thus, the interpretation of the spectra.

In summary, from the presented ex situ characterization, the following conclusions can be drawn.

- ALD2 presents Pt single ion sites at the WO_3 surface, as it is indicated by the applied X-ray spectroscopies and the absence of any segregated phase in the electron micrographs.
- ALD5 shows a separated solid phase in the electron micrographs and the presence of Pt^{4+} in the XP spectrum as well as a higher whiteline intensity in the HERFD-XANES spectra. This suggests the presence of single Pt ion sites as well as small oxidized Pt particles.
- ALD10 is expected to have only PtO_2 particles on the WO_3 surface, as only Pt^{4+} is found by XPS, and the electron micrographs show a separated phase
- ALD25 and ALD50 show very similar results, that is, a separate phase in the electron micrographs, which by XPS is assigned to both superficially oxidized Pt particles (Pt^0 and Pt^{2+}) and fully oxidized Pt (Pt^{4+}). The presence of partially oxidized Pt agrees with the HERFD-XANES spectra of ALD25.

Therefore, the following trend with an increasing number of ALD cycles can be determined. First, single Pt ion sites are formed on the surface (ALD2), followed by the coexistence of these single ion sites with very small, oxidized particles (ALD5), which then evolve into the dominant presence of entirely oxidized Pt particles (ALD10). However, further Pt deposition then leads to the formation of metallic particles that are superficially oxidized (ALD25 and ALD50).

The gas sensing performance at 300 °C of pristine and Pt-loaded WO_3 was studied for CO, acetone, toluene, NO_2, ethanol, and H_2 in different relative humidity backgrounds (5, 30, and 70% RH; see Figure S3). As shown in Figure 5, the presence of Pt on WO_3 significantly changes the response of the Pt-loaded materials toward the different analyte gases, namely, increasing the response to CO and H_2 in comparison to organic vapors like ethanol, toluene, and acetone. This is apparent when comparing the ratios of the sensor signals of CO and acetone (Figure S4). Pristine WO_3 shows by far a higher response to acetone than to CO. The highest ratio of the CO to acetone signal is observed for ALD5. The signal ratios of ALD2 are located between those of pristine WO_3 and ALD5. The other Pt-loaded samples, ALD10 to ALD50, show response ratios only slightly lower than the one of ALD5.

https://doi.org/10.1021/acs.jpcc.5c05000
J. Phys. Chem. C 2025, 129, 15301−15308

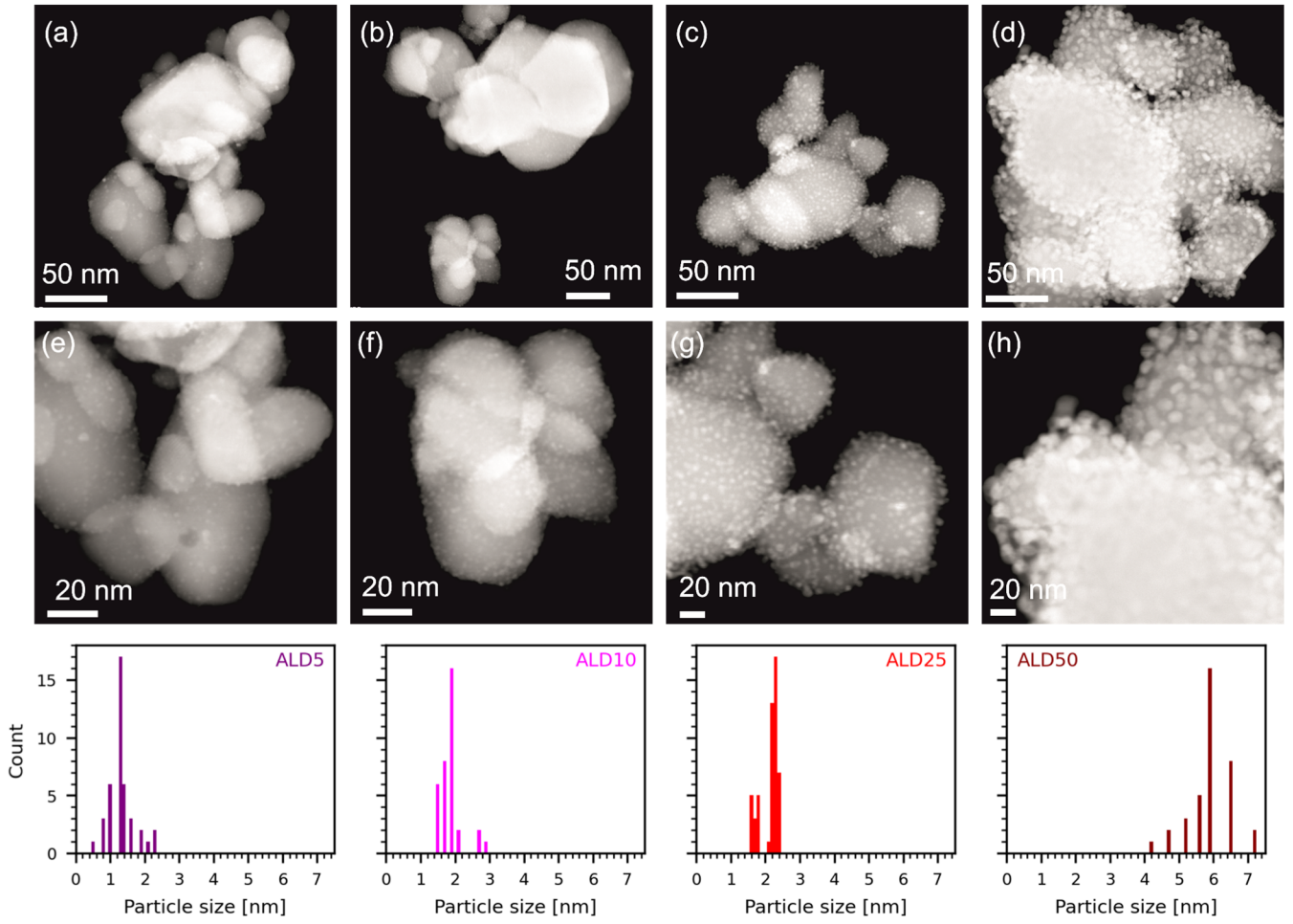

Figure 3. HAADF-STEM micrographs for ALD5 (a, e), ALD10 (b, f), ALD25 (c, g), and ALD50 (d, h) after calcination at different levels of magnification (top and middle rows) and the corresponding particle diameter distribution (bottom row). The HADDF-STEM micrographs before calcination are shown in Figure S2.

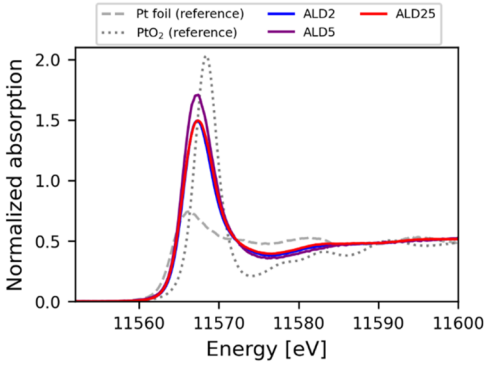

Figure 4. Pt L_3 HERFD-XANES spectra of ALD2 (blue), ALD5 (purple), and ALD25 (red) in 20%vol O_2 in He, at a sensor temperature of 300 °C and Pt foil (dashed) and PtO_2 (dotted) references at room temperature.

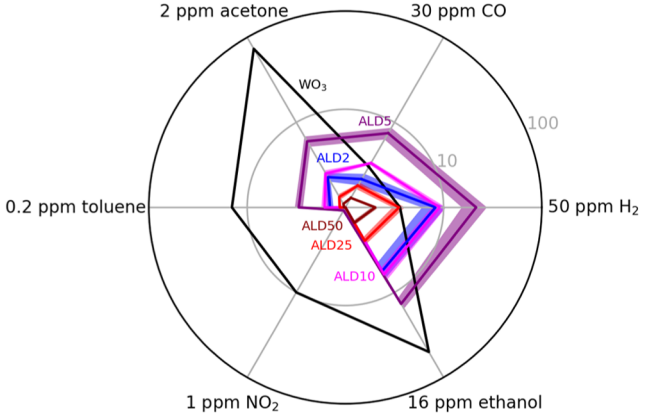

Figure 5. Sensor signals (R_{air}/R_{gas} or R_{NO2}/R_{air}) of pristine WO_3, ALD2, ALD5, ALD10, ALD25, and ALD50 in 5% RH and at a sensor temperature of 300 °C. The shaded areas for ALD-loaded sensors indicate error bars, calculated as the standard deviation of three independent samples. The gas sensing performance at different humidity levels is shown in Figure S3.

To gain further insight into the influence of the Pt loading on the electrical properties and the interaction with atmospheric oxygen, the resistances of all sensors were measured in pure N_2 and synthetic air at 300 °C (Figure 6, **top**). As previously reported, the presence of noble metal additives increases the sensor resistances measured in N_2 when compared to pristine SMOX, indicating a strong electronic coupling of the additives; the latter is due to electronic states related to single ion sites or Fermi-level coupling of additive clusters or particles at the SMOX surface.[11] ALD2 and ALD5 show the highest resistance in N_2, indicating the strongest electronic interaction of Pt loadings with WO_3. ALD10 shows a lower interaction, which is

https://doi.org/10.1021/acs.jpcc.5c05000
J. Phys. Chem. C 2025, 129, 15301−15308

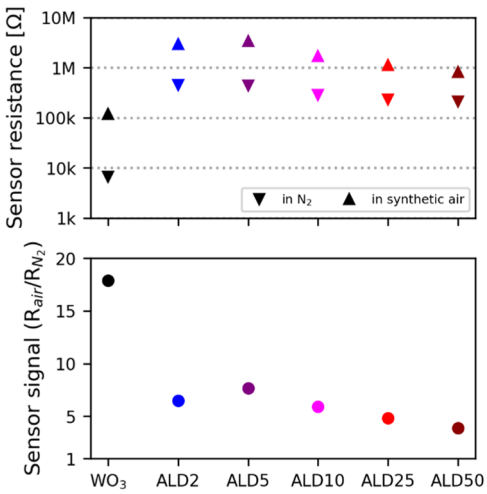

Figure 6. Sensor resistances in pure N_2 and synthetic air (top) and the calculated signals of ~20% O_2 (bottom) for WO_3 (black), ALD2 (blue), ALD5 (purple), ALD10 (magenta), ALD25 (red), and ALD50 (dark red) at a sensor temperature of 300 °C.

still higher than those of ALD25 and ALD50. This leads to the conclusion that the loadings from ALD2 to ALD5 and finally to ALD50 interact differently, which correlates with the different Pt structures found.

Based on the resistances in pure N_2 and synthetic air (Figure 6, **bottom**), sensor signals are calculated to quantify the effect of O_2. Pristine WO_3 shows the highest impact of the O_2 on the sensor resistance. Within the Pt-loaded samples, ALD5 presents the highest change in resistance due to the presence of oxygen, while ALD2, as well as ALD10 to ALD50, show lower O_2 signals, whereby ALD10 to ALD50 show a continuously decreasing trend. The trend seen for oxygen exposure correlates with the CO sensing performance of the Pt-loaded samples (Figure 5); that is expected since the detection of CO depends on its interaction of ionosorbed oxygen at the SMOX surface or additive structure, e.g., by its total or partial combustion.[6,7]

To further understand the observed trends with increasing number of ALD cycles, i.e., increasing Pt loading and changes in the nature of the Pt species, operando spectroscopic investigations were performed. ALD2, ALD5, and ALD25 were studied by operando XAS during CO sensing (Figure 7), and furthermore, all samples were studied by operando DRIFTS

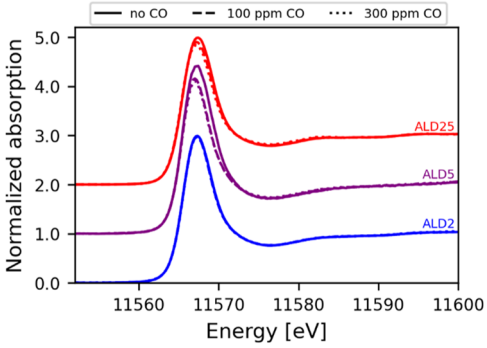

Figure 7. Operando Pt L_3 HERFD-XANES spectra of ALD2 (blue), ALD5 (purple), and ALD25 (red) in the absence of CO (solid line); 100 ppm of CO (dashed line) and 300 ppm of CO (dotted line) dosed in 20% O_2 in He at a sensor temperature of 300 °C. The recorded sensor signals are reported in Figure S5.

during CO sensing (Figure 8). The Pt L_3 HERFD-XANES spectra of ALD2 show no change upon exposure to 100 or 300

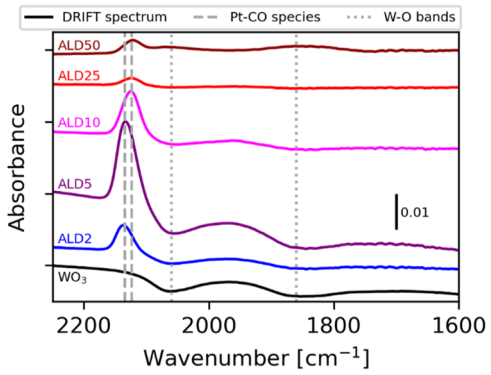

Figure 8. Operando DRIFT spectra of WO_3 (black), ALD2 (blue), ALD5 (purple), ALD10 (magenta), ALD25 (red), and ALD50 (dark red) for 100 ppm of CO dosed in dry air at a sensor temperature of 300 °C. The recorded sensor signals are reported in Figure S5.

ppm of CO. However, since still a change in resistance is observed (Figure S4), it can be assumed that single ion Pt sites are not changed during gas sensing and that the electrical effect stems from the reduction of the WO_3 surface instead. Indeed, an activation of lattice oxygen bound to Pt, as proposed for Pt-doped SnO_2, would explain the increased response to CO.[27] In contrast, ALD5 and ALD25 show a clear effect on the HERFD-XANES spectra: the whiteline is shifted to lower energies, and its intensity decreases due to Pt reduction, with this effect being more pronounced for ALD5. The distinct change in Pt L_3 whiteline suggests a significant change of the Pt loading by CO, which can be assigned to a reduction of oxidized Pt particles. The more pronounced reduction of Pt for ALD5 can be explained by the higher ratio of CO molecules with respect to the Pt sites at the surface as well as the better accessibility of Pt sites by gases on the smaller clusters of ALD5.

The understanding of the sensing is furthered by operando DRIFT spectroscopy. All recorded DRIFT spectra show two bands at 2060 and 1860 cm^{-1} (Figure 8, dotted gray lines) assigned to the W═O vibrational mode.[6] The decreasing W═O bands in pristine WO_3 indicate the reduction of the surface due to the oxidation of CO with lattice oxygen, as expected from previous reports.[6,7] This behavior is observed, to a lesser extent, for ALD2 and ALD5, further decreasing with increasing Pt loading, until for ALD50, an increase in the W═O bands, i.e., oxidation of the surface, is observed. The latter effect has been previously observed for highly noble metal-loaded SMOX and is explained by enhanced oxygen ionosorption, which is enabled by additional electrons released from the heterojunctions back into the SMOX.[28]

In addition to these, the Pt-loaded samples show bands that are assigned to the CO species adsorbed to Pt sites (Figure 8, dashed gray lines). ALD2 and ALD5 show bands at 2137 and 2134 cm^{-1}, indicating the presence of oxidized Pt^{2+} sites at the surface.[29] Based on the other material characterization, this band is assigned to the Pt single ion sites at the WO_3 surface. The DRIFT spectra of ALD10 to ALD50 present a band at 2123 to 2121 cm^{-1}, which can be assigned to CO adsorbed on ionic Pt species found in superficially oxidized metallic Pt particles supported on Al_2O_3.[30] None of the Pt-loaded samples show a band around 2066 cm^{-1} and, thus, the presence of any carbonyl species adsorbed to metallic Pt sites can be excluded.[30,31] The

https://doi.org/10.1021/acs.jpcc.5c05000
J. Phys. Chem. C 2025, 129, 15301−15308

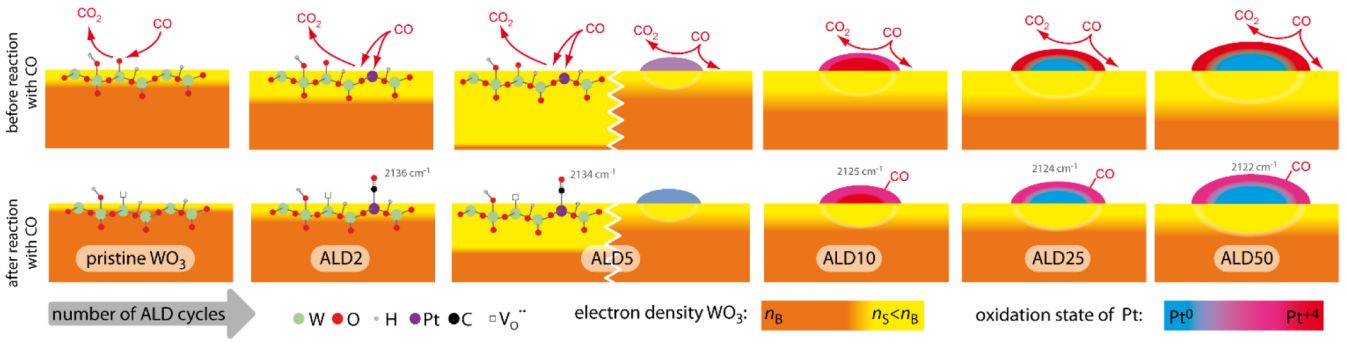

Figure 9. Schematic representation of the WO_3 sensing material with respect to the amount of platinum deposited. The orange-shaded areas correspond to regions with an electron density like in the bulk of WO_3 (n_b); the yellow shaded areas correspond to electron-depleted regions, i.e., the surface electron concentration being lower as in the bulk ($n_s < n_b$). The top row illustrates the state of the surface and sites for the reaction of CO: up to ALD5, the interaction with single oxygen and platinum sites is dominant, while at a higher number of ALD cycles, the growth and composition of Pt clusters is shown on a macroscopic scale. In the bottom row, the effect of CO on both WO_3 and Pt is shown.

analysis of the Pt carbonyl species observed by DRIFTS revealed the presence of two distinctly different Pt surface types: one clearly indicating the presence of Pt single sites at the surface in the case of ALD2 and ALD5, and another one for ALD10 to ALD50, where more reduced Pt species are found, e.g., as observed for oxidized sites on metallic particles. Furthermore, the trend observed with increasing Pt loading for the W═O bands suggests that, with increasing Pt coverage, less CO interacts with the WO_3, i.e., the surface chemistry is further shifted to the Pt loadings.

Based on the comprehensive material characterization and operando spectroscopic investigations, the structure and function of the different samples are summarized, as shown in Figure 9. For the lowest loading ALD2, Pt is solely present in the form of single ion sites, which play a double role. On the one hand, they are acceptor levels, which is indicated by the very significant increase of the resistance in N_2. The deficit of free electrons available results in fewer chemisorbed oxygen ions and, as a consequence of that, fewer reaction partners are available for the reaction with CO. This is manifested by the less pronounced decrease of the W═O bands when compared to the unloaded material. On the other hand, the Pt ion sites act as adsorption or reactive sites and only locally increase the reactivity of lattice oxygen, partially compensating for the aforementioned lower reactivity of the WO_3 surface for certain gases like CO or H_2.

ALD5 shows the coexistence of different Pt species. Material characterization by electron microscopy and operando HERFD-XANES clearly indicates the presence of oxidized Pt particles. In contrast, the operando DRIFT spectrum reveals the presence of single ion sites. Thus, in addition to the single ion Pt sites, small clusters are reduced by CO and, via electronic coupling (Fermi-level control), cause a decrease of the sensor resistance in the presence of reducing gases. ALD5 represents the case in which the two effects of the surface ionic sites and small oxidized clusters synergistically combine to increase the sensor performance.

Further increasing the Pt loading (ALD10) results in the surface being dominated by oxidized Pt particles, which are larger than those observed for ALD5. The efficiency of the sensitization by Fermi-level control decreases for larger particles, due to the nonreducible part of the particle at the particle-WO_3 interface shielding electronic changes of the Pt particle surface from the supporting WO_3.[11] In addition to the shielding, the decrease in sensor signals is also caused by the higher coverage of the surface with reactive Pt particles. Since the same amount of analyte reacts with more Pt sites, these are more easily reoxidized, which reduces the net change in particle composition and, thus, the gas sensing effect. Hence, the sensor signals are found to be lower than those for ALD5.

For even higher Pt loadings (ALD25 and ALD50), Pt forms predominantly metallic particles with an oxidized surface. The presence of a metallic core in the particles leads to even stronger electronic shielding, which hinders a Fermi-level-control mechanism and results in a further decrease in sensor signals. As with ALD10, the decrease in sensor signals is also favored by the increasing coverage of the surface with reactive Pt particles.

SUMMARY

ALD has been successfully used on already deposited SMOX gas sensing layers to form different Pt coverages, along with different Pt structures on WO_3. This clearly demonstrates the versatility of the ALD method for depositing noble metals onto metal oxide surfaces. ALD hence allows Pt to be efficiently deposited on the entire surface accessible to gases, thus potentially reducing the amount of noble metals required to change the gas sensing properties of the supporting SMOX.

In summary, three crucial aspects can be derived from this study for the role of noble metal additives in SMOX gas sensing materials:

- Single ion sites play a double role acting as electronic states, in the case of Pt ions in WO_3 as acceptor state, as well as local adsorption and reactions sites, which enhance the sensor response to certain gases.
- Fully oxidized and preferentially small clusters or particles generally exhibit good reactivity toward analyte gases and can effectively convert this reactivity into a change in resistance via the Fermi-level control mechanism and, thus, into a sensor signal.
- Partially oxidized metallic clusters may still be highly reactive; however, due to the shielding of the electronic interaction by the metallic core, a Fermi-level control mechanism is less effective or even no longer possible.

Hence, it can be concluded that the most effective sensitization of SMOX can be achieved by single ion sites or extremely small oxide particles. As shown for ALD5, the presence of single ion sites, an effective Fermi-level control mechanism, and a synergistic combination of both effects on the sensing properties are not mutually exclusive. Thus, an in-depth investigation of the transition from single Pt sites to clusters and

https://doi.org/10.1021/acs.jpcc.5c05000
J. Phys. Chem. C 2025, 129, 15301−15308

particles will be of great interest to enable the knowledge-based design of highly efficient SMOX gas sensor materials.

■ ASSOCIATED CONTENT

Supporting Information

The Supporting Information is available free of charge at https://pubs.acs.org/doi/10.1021/acs.jpcc.5c05000.

XP spectra recorded prior to calcination, STEM micrographs and particle size distribution before calcination, ratio of CO and acetone sensor signals for the studied samples, and sensor signals of CO for different operando methods (PDF)

■ AUTHOR INFORMATION

Corresponding Author

Nicolae Barsan − *Institute of Physical and Theoretical Chemistry (IPTC), University of Tuebingen, Tuebingen 72076, Germany; Center for Light-Matter Interaction, Sensors & Analytics (LISA+), University of Tuebingen, Tuebingen 72076, Germany; Faculty of Advanced Science and Technology (FAST), Kumamoto University, Kumamoto 860-8555, Japan;* orcid.org/0000-0001-6718-9889; Phone: +49 7071 29 78761; Email: nb@ipc.uni-tuebingen.de

Authors

David Degler − *Department of Applied Sciences and Mechatronics, University of Applied Science Munich, Munich 80335, Germany*

Ugur Geyik − *Institute of Physical and Theoretical Chemistry (IPTC), University of Tuebingen, Tuebingen 72076, Germany; Center for Light-Matter Interaction, Sensors & Analytics (LISA+), University of Tuebingen, Tuebingen 72076, Germany*

Benjamin Junker-Reiss − *Institute of Physical and Theoretical Chemistry (IPTC), University of Tuebingen, Tuebingen 72076, Germany; Center for Light-Matter Interaction, Sensors & Analytics (LISA+), University of Tuebingen, Tuebingen 72076, Germany;* orcid.org/0000-0002-2229-0534

Muhammad Hamid Raza − *Department of Chemistry, Center for the Science of Materials Berlin, Humboldt-Universität zu Berlin, Berlin 12489, Germany; Center for the Science of Materials Berlin, Humboldt-Universität zu Berlin, Berlin 12489, Germany; PVcomB, Helmholtz-Zentrum Berlin für Materialien und Energie GmbH (HZB), Berlin 12489, Germany;* orcid.org/0000-0003-0061-5139

Patrick Amsalem − *Institut für Physik and the Center for the Science of Materials Berlin, Humboldt-Universität zu Berlin, Berlin 12489, Germany;* orcid.org/0000-0002-7330-2451

Norbert Koch − *Institut für Physik and the Center for the Science of Materials Berlin, Humboldt-Universität zu Berlin, Berlin 12489, Germany;* orcid.org/0000-0002-6042-6447

Blanka Detlefs − *European Synchrotron Radiation Facility, Grenoble 38043, France;* orcid.org/0000-0002-9768-647X

Nicola Pinna − *Department of Chemistry, Center for the Science of Materials Berlin, Humboldt-Universität zu Berlin, Berlin 12489, Germany; Center for the Science of Materials Berlin, Humboldt-Universität zu Berlin, Berlin 12489, Germany;* orcid.org/0000-0003-1273-803X

Udo Weimar − *Institute of Physical and Theoretical Chemistry (IPTC), University of Tuebingen, Tuebingen 72076, Germany; Center for Light-Matter Interaction, Sensors & Analytics (LISA+), University of Tuebingen, Tuebingen 72076, Germany;* orcid.org/0000-0003-2354-0432

Complete contact information is available at: https://pubs.acs.org/10.1021/acs.jpcc.5c05000

Author Contributions

The manuscript was written through contributions of all authors. D.D. planned and evaluated the XANES investigations, merged the various results, and was responsible for writing the manuscript. U.G. prepared the pristine samples and planned, conducted, and evaluated the sensing performance, DRIFTS, and XANES investigations. B.J.-R. prepared and conducted XANES investigations and assisted in writing the manuscript. M.H.R. developed and optimized the Pt ALD process, deposited Pt on sensors, analyzed TEM data, and helped with XPS data analysis and discussion on sensing results. P.A. and N.K. measured and analyzed XPS data. B.D. was the local contact for the synchrotron-based measurements and supported all works carried out at the ESRF. N.P., U.W., and N.B. supervised the study. All authors contributed to the discussion of the results and the correction of the manuscript. All authors have given approval to the final version of the manuscript.

Notes

The authors declare no competing financial interest.

■ ACKNOWLEDGMENTS

The authors acknowledge the European Synchrotron Radiation Facility (ESRF) for the provision of synchrotron radiation facilities under proposal number CH-6029 (doi: 10.15151/ESRF-ES-650701946), and they would like to thank the staff of ESRF's beamline ID26 for assistance and support during the beamtime.

■ ABBREVIATIONS

ALD, atomic layer deposition
Cp, cyclopentadienyl
DRIFTS, diffuse reflectance infrared Fourier transform spectroscopy
HAADF-STEM, high-angle annular dark-field scanning transmission electron microscopy
HERFD, high-energy-resolved fluorescence detection
RH, relative humidity
SMOX, semiconducting metal oxide
XANES, X-ray absorption near edge structure
XAS, X-ray absorption spectroscopy
XPS, X-ray photoelectron spectroscopy

■ REFERENCES

(1) Barsan, N.; Koziej, D.; Weimar, U. Metal Oxide-Based Gas Sensor Research: How To? *Sens. Actuators, B* **2007**, *121* (1), 18−35.

(2) Yamazoe, N.; Sakai, G.; Shimanoe, K. Oxide Semiconductor Gas Sensors. *Catal. Surv. Asia* **2003**, *7* (1), 63−75.

(3) Neri, G. First Fifty Years of Chemoresistive Gas Sensors. *Chemosensors* **2015**, *3* (1), 1−20.

(4) Degler, D.; Wicker, S.; Weimar, U.; Barsan, N. Identifying the Active Oxygen Species in SnO2 Based Gas Sensing Materials: An Operando IR Spectrsocopy Study. *J. Phys. Chem. C* **2015**, *119* (21), 11792−11799.

(5) Sänze, S.; Hess, C. Ethanol Gas Sensing by Indium Oxide: An Operando Spectroscopic Raman-FTIR Study. *J. Phys. Chem. C* **2014**, *118* (44), 25603−25613.

(6) Hübner, M.; Simion, C. E.; Haensch, A.; Barsan, N.; Weimar, U. CO Sensing Mechanism with WO3 Based Gas Sensors. *Sens. Actuators, B* **2010**, *151* (1), 103−106.
(7) Staerz, A.; Somacescu, S.; Epifani, M.; Kida, T.; Weimar, U.; Barsan, N. WO3-Based Gas Sensors: Identifying Inherent Qualities and Understanding the Sensing Mechanism. *ACS Sens.* **2020**, *5* (6), 1624−1633.
(8) Schmitt, E. A.; Krott, M.; Epifani, M.; Suematsu, K.; Weimar, U.; Barsan, N. Volatile Organic Compound Sensing with WO3-Based Gas Sensors: Surface Chemistry Basics. *J. Phys. Chem. C* **2024**, *128* (4), 1633−1643.
(9) Barsan, N.; Weimar, U. Conduction Model of Metal Oxide Gas Sensors. *Growth (Lakeland)* **2001**, *7*, 143−167.
(10) Müller, S. A.; Degler, D.; Feldmann, C.; Türk, M.; Moos, R.; Fink, K.; Studt, F.; Gerthsen, D.; Bârsan, N.; Grunwaldt, J. D. Exploiting Synergies in Catalysis and Gas Sensing Using Noble Metal-Loaded Oxide Composites. *ChemCatChem* **2018**, *10* (5), 864−880.
(11) Degler, D.; Weimar, U.; Barsan, N. Current Understanding of the Fundamental Mechanisms of Doped and Loaded Semiconducting Metal-Oxide-Based Gas Sensing Materials. *ACS Sens.* **2019**, *4* (9), 2228−2249.
(12) Dendooven, J.; Ramachandran, R. K.; Solano, E.; Kurttepeli, M.; Geerts, L.; Heremans, G.; Rongé, J.; Minjauw, M. M.; Dobbelaere, T.; Devloo-Casier, K.; et al. Independent Tuning of Size and Coverage of Supported Pt Nanoparticles Using Atomic Layer Deposition. *Nat. Commun.* **2017**, *8* (1), No. 1074.
(13) Raza, M. H.; Movlaee, K.; Leonardi, S. G.; Barsan, N.; Neri, G.; Pinna, N. Gas Sensing of NiO-SCCNT Core−Shell Heterostructures: Optimization by Radial Modulation of the Hole-Accumulation Layer. *Adv. Funct. Mater.* **2020**, *30* (6), No. 1906874.
(14) Bârsan, N.; Weimar, U. Understanding the Fundamental Principles of Metal Oxide Based Gas Sensors; the Example of CO Sensing with SnO2 Sensors in the Presence of Humidity. *J. Phys.:Condens. Matter* **2003**, *15* (20), R813−R839.
(15) Glatzel, P.; Harris, A.; Marion, P.; Sikora, M.; Weng, T. C.; Guilloud, C.; Lafuerza, S.; ovezzi, M.; Detlefs, B.; Ducotté, L. The Five-Analyzer Point-to-Point Scanning Crystal Spectrometer at ESRF ID26. *J. Synchrotron Radiat.* **2021**, *28*, 362−371.
(16) Newville, M. Larch: An Analysis Package for XAFS and Related Spectroscopies. *J. Phys. Conf. Ser.* **2013**, *430* (1), No. 012007.
(17) Grossmann, K.; Pavelko, R. G.; Barsan, N.; Weimar, U. Interplay of H 2, Water Vapor and Oxygenat the Surface of SnO 2 Based Gas Sensors - An Operando Investigation Utilizing Deuterated Gases. *Sens. Actuators, B* **2012**, *166−167*, 787−793.
(18) Bera, P.; Priolkar, K. R.; Gayen, A.; Sarode, P. R.; Hegde, M. S.; Emura, S.; Kumashiro, R.; Jayaram, V.; Subbanna, G. N. Ionic Dispersion of Pt over CeO2 by the Combustion Method: Structural Investigation by XRD, TEM, XPS, and EXAFS. *Chem. Mater.* **2003**, *15* (10), 2049−2060.
(19) Park, J.; Lee, S.; Kim, H. E.; Cho, A.; Kim, S.; Ye, Y.; Han, J. W.; Lee, H.; Jang, J. H.; Lee, J. Investigation of the Support Effect in Atomically Dispersed Pt on WO3−x for Utilization of Pt in the Hydrogen Evolution Reaction. *Angew. Chem., Int. Ed.* **2019**, *58* (45), 16038−16042.
(20) Vovk, E. I.; Kalinkin, A. V.; Smirnov, M. Y.; Klembovskii, I. O.; Bukhtiyarov, V. I. XPS Study of Stability and Reactivity of Oxidized Pt Nanoparticles Supported on TiO2. *J. Phys. Chem. C* **2017**, *121* (32), 17297−17304.
(21) Shin, S.; Kim, J.; Park, S.; Kim, H. E.; Sung, Y. E.; Lee, H. Changes in the Oxidation State of Pt Single-Atom Catalysts upon Removal of Chloride Ligands and Their Effect for Electrochemical Reactions. *Chem. Commun.* **2019**, *55* (45), 6389−6392.
(22) Maurer, F.; Jelic, J.; Wang, J.; Gänzler, A.; Dolcet, P.; Wöll, C.; Wang, Y.; Studt, F.; Casapu, M.; Grunwaldt, J. D. Tracking the Formation, Fate and Consequence for Catalytic Activity of Pt Single Sites on CeO2. *Nat. Catal.* **2020**, *3* (10), 824−833.
(23) Chen, Y.; Ji, S.; Sun, W.; Chen, W.; Dong, J.; Wen, J.; Zhang, J.; Li, Z.; Zheng, L.; Chen, C.; et al. Discovering Partially Charged Single-Atom Pt for Enhanced Anti-Markovnikov Alkene Hydrosilylation. *J. Am. Chem. Soc.* **2018**, *140* (24), 7407−7410.
(24) Hübner, M.; Koziej, D.; Bauer, M.; Barsan, N.; Kvashnina, K.; Rossell, M. D.; Weimar, U.; Grunwaldt, J. D. The Structure and Behavior of Platinum in SnO2-Based Sensors under Working Conditions. *Angew. Chem., Int. Ed.* **2011**, *50* (12), 2841−2844.
(25) Degler, D. Trends and Advances in the Characterization of Gas Sensing Materials Based on Semiconducting Oxides. *Sensors (Switzerland)* **2018**, *18* (10), No. 3544.
(26) Gänzler, A. M.; Casapu, M.; Doronkin, D. E.; Maurer, F.; Lott, P.; Glatzel, P.; Votsmeier, M.; Deutschmann, O.; Grunwaldt, J. D. Unravelling the Different Reaction Pathways for Low Temperature CO Oxidation on Pt/CeO2 and Pt/Al2O3 by Spatially Resolved Structure-Activity Correlations. *J. Phys. Chem. Lett.* **2019**, *10* (24), 7698−7705.
(27) Degler, D.; Pereira De Carvalho, H. W.; Kvashnina, K.; Grunwaldt, J. D.; Weimar, U.; Barsan, N. Structure and Chemistry of Surface-Doped Pt:SnO2 Gas Sensing Materials. *RSC Adv.* **2016**, *6* (34), 28149−28155.
(28) Staerz, A.; Boehme, I.; Degler, D.; Bahri, M.; Doronkin, D. E.; Zimina, A.; Brinkmann, H.; Herrmann, S.; Junker, B.; Ersen, O.; et al. Rhodium Oxide Surface-Loaded Gas Sensors. *Nanomaterials* **2018**, *8* (11), 1−17.
(29) Ivanova, E.; Mihaylov, M.; Thibault-Starzyk, F.; Daturi, M.; Hadjiivanov, K. FTIR Spectroscopy Study of CO and NO Adsorption and Co-Adsorption on Pt/TiO2. *J. Mol. Catal. A:Chem.* **2007**, *274* (1−2), 179−184.
(30) Boubnov, A.; Gänzler, A.; Conrad, S.; Casapu, M.; Grunwaldt, J. D. Oscillatory CO Oxidation over Pt/Al2O3 Catalysts Studied by in Situ XAS and DRIFTS. *Top. Catal.* **2013**, *56* (1−8), 333−338.
(31) Meunier, F. C. Relevance of IR Spectroscopy of Adsorbed CO for the Characterization of Heterogeneous Catalysts Containing Isolated Atoms. *J. Phys. Chem. C* **2021**, *125* (40), 21810−21823.

https://doi.org/10.1021/acs.jpcc.5c05000
J. Phys. Chem. C 2025, 129, 15301−15308